

Laser Wakefield Electron Acceleration with Polarization-Dependent Ionization Injection

Mohammad Rezaei-Pandari^{1,2}, Mohammad Mirzaie^{1,2,*}, Calin Ioan Hojbota^{1,2}, Tae Gyu Pak^{1,2,3}, Sang Beom Kim,^{2,3} Geon Woo Lee,^{2,3} Reza Massudi,¹ Ali Reza Niknam,¹ Seong Ku Lee,^{2,4}, Ki-Yong Kim^{1,2,3,5,†} and Chang Hee Nam^{2,3}

¹ *Laser and Plasma Research Institute, Shahid Beheshti University, 1983969411, Tehran, Iran*

² *Center for Relativistic Laser Science (CoReLS), Institute for Basic Science, Gwangju 61005, Republic of Korea*

³ *Department of Physics and Photon Science, Gwangju Institute of Science and Technology, Gwangju 61005, Republic of Korea*

⁴ *Advanced Photonics Research Institute, Gwangju Institute of Science and Technology, Gwangju, 61005, Republic of Korea*

⁵ *Institute for Research in Electronics and Applied Physics and Department of Physics, University of Maryland, College Park, Maryland 20742, USA*

(Received 9 March 2023; revised 13 June 2023; accepted 4 August 2023; published 13 September 2023)

The effect of laser polarization on the laser wakefield acceleration (LWFA) of electrons has been investigated in the bubble regime, in particular when assisted by ionization injection. By utilizing linear and circular laser polarizations, we discover that circular polarization leads to a dramatic increase in the electron reproducibility rate and also increases the electron charge and beam divergence, while linear polarization yields higher electron peak energy and more stable beam pointing. Our experimental findings are also supported by three-dimensional particle-in-cell simulations. Our study highlights the potential of laser polarization as a simple and effective tool in controlling LWFA and electron-beam properties depending on applications.

DOI: 10.1103/PhysRevApplied.20.034026

I. INTRODUCTION

The technological advancement of high-power femtosecond lasers [1] has enabled a rapid development of laser-plasma-based accelerators [2]. These accelerators, also known as laser wakefield accelerators, are considered a new generation of compact accelerators with accelerating electric fields as high as 100 GeV/m, due to the large space charge occurring inside the plasma [3–6]. In such an accelerator, a high-intensity laser pulse propagates through a gaseous medium and ionizes the constituent atoms and molecules, forming a plasma. Due to the ponderomotive force exerted by the intense laser pulse, a large-amplitude oscillating (and copropagating) density perturbation, known as a wakefield, is formed in the plasma behind the laser pulse [4,6,7]. This wakefield can effectively accelerate electrons to a multi-giga-electronvolt (multi-GeV) energy level over a short distance (approximately centimeters). The high-energy electron beams produced by laser wakefield acceleration (LWFA) can be also utilized as secondary radiation sources for gamma rays [8],

x rays [9], betatron x-ray radiation [10], and even terahertz (THz) radiation [11].

In the LWFA scheme, the laser-plasma interaction can be highly nonlinear and relativistic. The transverse oscillatory motion of electrons becomes relativistic when the normalized laser vector potential, $a_0 = eE_0/(m_e\omega_l c)$, is greater than one, where e , E_0 , m_e , ω_l , and c are the electron charge, the electric field amplitude, the electron mass, the laser angular frequency, and the speed of light, respectively. Such an intense laser pulse can create an electron-free region behind it, known as the bubble (or cavitation) [4,12]. When electrons are trapped in the bubble, they can be accelerated by the wakefield due to the longitudinal electric field formed inside the bubble. Once the wakefield is established, the primary concern is how to trap electrons and control their injection. In general, the electrons should move faster than the phase velocity of the plasma wave in order to be trapped in the wakefield [13–15]. Based on this concept, several injection schemes have been proposed and demonstrated so far, including ionization injection [16,17], external injection [18,19], self-injection [20–22], down-ramp injection [23], shock injection [24], and nanoparticle-assisted injection [25]. Among these, self-injection and ionization

*Corresponding author. mirzaie@ibs.re.kr

†Corresponding author. kykim@umd.edu

injection in the bubble regime have been most popularly exploited.

According to the linear wakefield model, the gradient of the laser intensity ($\nabla I \sim \nabla \alpha_0^2$) plays a crucial role in the bubble generation and electron trapping, while laser polarization does not play a direct role [4,26]. Surprisingly, Ma *et al.* have recently shown that self-injection is greatly affected by the polarization of a laser pulse interacting with a target gas [27]. This is because the ionization of background atoms or molecules strongly depends on laser polarization and the initial momentum distribution of ionized electrons is also polarization sensitive, owing to above-threshold ionization (ATI) [27]. In particular, the threshold for self-injection becomes lower with circular polarization (CP) than with linear polarization (LP). This is because the initial momentum of electrons ionized by a CP laser is larger compared to LP. Besides, when the laser energy and the electron density are sufficiently high, the electron charge injected in the CP case can be an order of magnitude larger than that in the LP case under the same plasma conditions [27]. Furthermore, the charge of injected electrons is also affected by the wavelength of a driver laser [28]. This self-injection scenario, however, cannot be arbitrarily controlled in real experiments, unlike the ionization-injection method [14,16,27,29].

In the ionization-injection scheme, a low- Z gas, e.g., hydrogen or helium, doped with a small amount of high- Z gas such as nitrogen or argon, is used as a target medium [30]. In general, electron injection is governed by the ionization energy of gas species and laser intensity. This in turn controls the resulting electron-beam energy spread, divergence, and charge [31,32]. As the ionization process depends on the polarization of the electric field, the polarization of an incident laser pulse can be utilized together

with ionization injection for further control of ionization and consequent electron-beam properties.

In this paper, we report an experimental and simulation study on the acceleration of electrons by polarization-dependent LWFA with ionization injection. This study investigates the effects of laser polarization (LP versus CP) on the properties of electron beams, including beam reproducibility, pointing fluctuation, divergence, charge, and energy. A numerical study based on three-dimensional (3D) particle-in-cell (PIC) simulations is also presented for a comprehensive understanding of polarization-sensitive LWFA, when driven with and without ionization injection.

II. RESULTS AND DISCUSSION

Our experiment was performed at the Center for Relativistic Laser Science (CoReLS) using a 150-TW Ti:sapphire laser ($\lambda = 800$ nm, $\tau = 25$ fs). The experimental scheme is shown in Fig. 1. An $f/23$ concave mirror (CM) focused the laser pulses onto a gas jet. The laser energy before compression was 3.9 ± 0.2 J and the wave front was corrected by a deformable mirror (DM) (AKA OPTICS DM2-60-32) and monitored by a wave-front sensor (Phasics SID4-GE). In addition, the DM was adjusted to move the focal-spot position by applying constant voltages to all DM segments, typically yielding approximately 0.225 mm/V. After optimization by the DM, the energy in the Airy disk was 30%, with a focal spot size of 25 μm in a full width at half maximum (FWHM) or $w_0 = 21 \mu\text{m}$ (at $1/e^2$ in intensity) at the target. This provides a peak laser intensity of $4.0 \times 10^{18} \text{ W/cm}^2$ with $a_0 = 1.4$. In this experiment, an ultrathin quarter-wave plate ($\lambda/4$) was used before the CM to switch the laser polarization between LP and CP. In the case of LP, the laser is polarized in the horizontal (x) direction in Fig. 1.

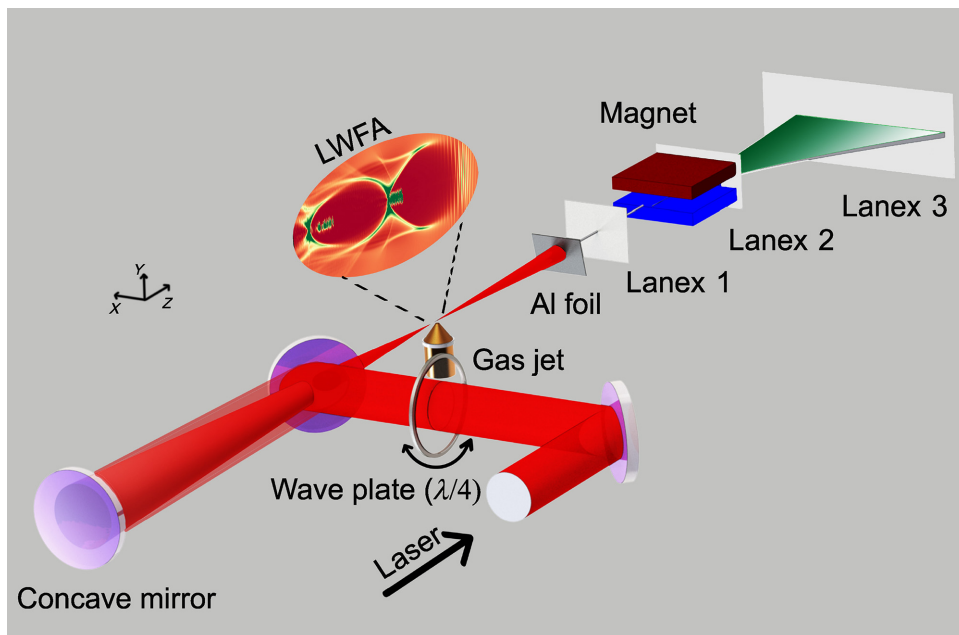


FIG. 1. The experimental scheme. A laser pulse (red) is focused onto the gas jet by a concave mirror for laser wakefield acceleration (LWFA). A quarter-wave plate ($\lambda/4$) is used to control the laser polarization. The resulting electron-beam profile is recorded using the scintillation screen Lanex 1 and the electron spectrum is recorded using the Lanex screens 2 and 3.

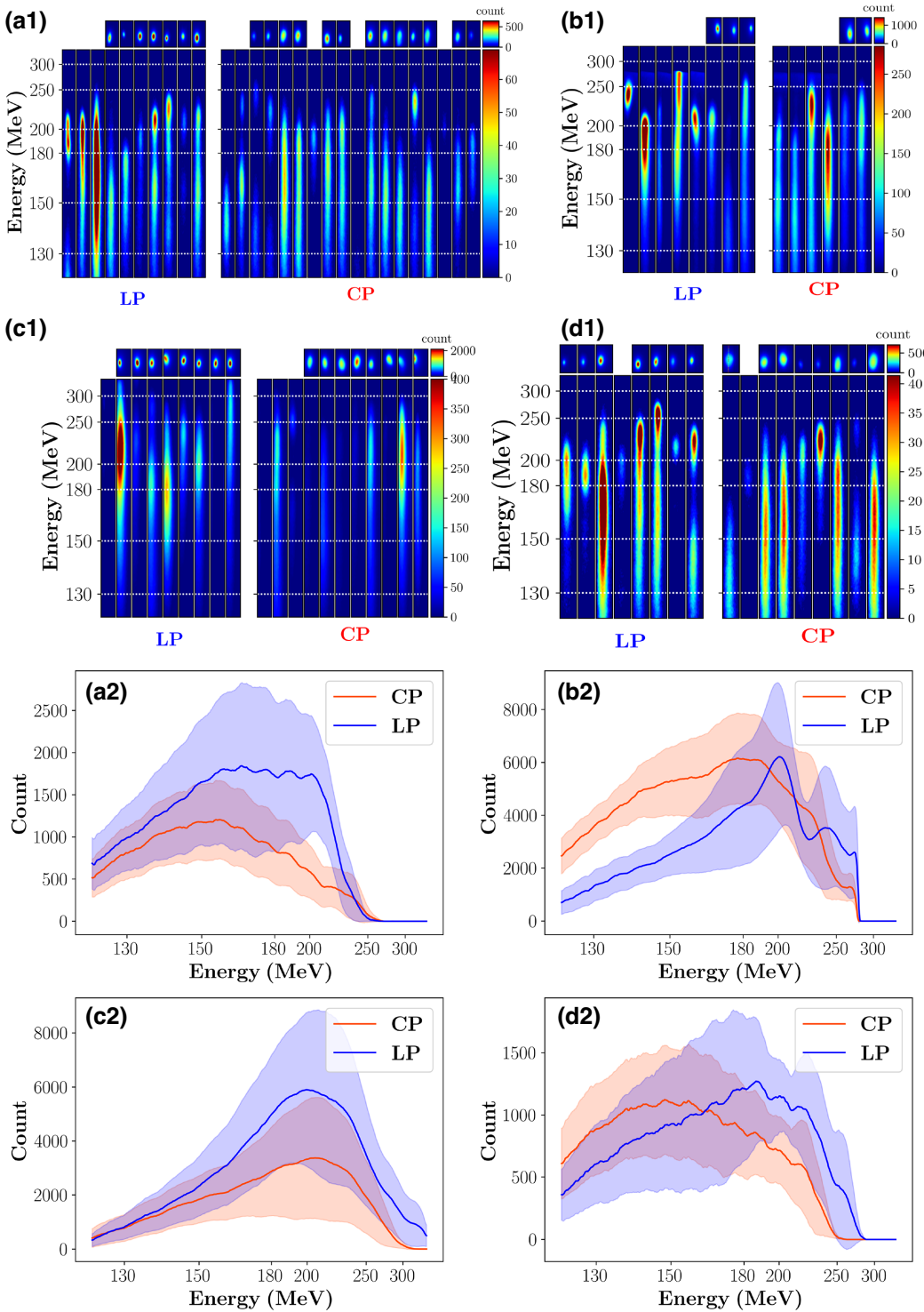


FIG. 2. Individual electron energy spectra [(a1), (b1), (c1), and (d1)] and averaged spectra [(a2), (b2), (c2), and (d2)] recorded on Lanex 3 for linearly polarized (LP) and circularly polarized (CP) laser pulses for a plasma density of ($n_e \times 10^{18} \text{ cm}^{-3}$) and a focal displacement (FD) of: (a) FD = 1.8 mm, $n_e = 5.4$; (b) FD = 5.6 mm, $n_e = 5.8$; (c) FD = 2.7 mm, $n_e = 4.8$; and (d) FD = 2.0 mm, $n_e = 5.4$. FD = 0 refers to the laser vacuum focal position at the entrance edge of the gas jet. The long and short color bars [(a1), (b1), (c1), and (d1)] are on different scales. A summary of the electron-beam properties is shown in Table I.

In the gas-jet setup, a cylindrical nozzle with a 4-mm inner diameter was used in a pulsed mode with an opening time of 10 ms. The gas backing pressure

varied in the range of 7–28 bar, providing gas densities of $0.8\text{--}3.9 \times 10^{18} \text{ cm}^{-3}$, measured with an interferometric method (see Fig. S1 in the Supplemental Material [33]).

We used a helium gas mixed with 3% nitrogen (He–3% N₂) for ionization injection. The focal point of the laser was located at the center and 2 mm above the orifice of the gas nozzle. After the interaction, thin Al foils were used to block the laser beam (see Fig. 1). The electron beam generated by LWFA was characterized using three scintillating Lanex (Kodak) screens. The profile, pointing, divergence, and relative charge of the electron beam were recorded using Lanex 1. The energy of the electron beam was measured with an electron spectrometer consisting of a 0.9-T dipole magnet, which disperses the electron beam on Lanex screens 2 and 3. This three-screen setup was adopted to minimize the error in measuring the electron-beam energy and correct for beam-pointing offsets [34]. The two screens can detect electrons in the energy range of 120–350 MeV and 150–400 MeV, respectively. The electron charge was determined by using an imaging plate (IP) from Fujifilm BAS-SR 2025, placed on top of Lanex 3. The IP was exposed to one shot and then scanned by a Fujifilm BAS5000 scanner. The charge was estimated by considering the photostimulated luminescence (PSL) coefficient, the energy dependence of PSL, and the time elapsed after the exposure [35,36].

We started with LP and scanned the plasma density by changing the gas backing pressure. We also optimized the laser focal position by adjusting the dc voltages applied to the DM to obtain an electron signal and find optimal parameters and then we investigated the influence of laser polarization on LWFA. First, we select four data sets as shown in Fig. 2 and summarized in Table I. They show successful shots taken with LP and CP under the same experimental parameters (i.e., gas backing pressure and laser focal position), selected from a total of 335 shots.

Figure 2 and Table I show that LP provides higher peak electron energies than CP in all cases (17% higher on average and 30% higher in case “D”). This is due to polarization-dependent ionization injection, in which the electrons ionized from the *K* shell of nitrogen (N⁶⁺) are born earlier in time under LP than under CP and are injected close to the back of the bubble so that they experience the stronger accelerating fields. This is detailed in Sec. III.

Another important parameter is the electron-beam-pointing fluctuation. Figure 3(a) shows variations in the electron-beam pointing observed on Lanex 1. For LP, the standard deviation of the beam-pointing fluctuation was found to be $\Delta\theta_x = 3.0 \pm 0.2$ mrad and $\Delta\theta_y = 2.2 \pm 0.1$ mrad in the *x* and *y* directions, respectively. However, after switching to CP, the standard deviation increased to $\Delta\theta_x = 3.5 \pm 0.3$ mrad and $\Delta\theta_y = 2.7 \pm 0.2$ mrad. This indicates that the beam-pointing fluctuation is slightly higher for CP compared to LP. Furthermore, as seen in Table I and Fig. 3(b), the beam-divergence angle (ϕ_x and

TABLE I. A summary of the electron-beam properties shown in Fig. 2.

Case	n_e ($\times 10^{18}$ cm ⁻³)	Number of shots on Lanex 1						Count on Lanex 1 (a.u.)						ϕ_x on Lanex 1 (mrad)						ϕ_y on Lanex 1 (mrad)						Charge on Lanex 3 (pC)						Peak of energy on Lanex 3 (MeV)					
		LP			CP			LP			CP			LP			CP			LP			CP			LP			CP			LP			CP		
		LP	CP	LP	CP	LP	CP	LP	CP	LP	CP	LP	CP	LP	CP	LP	CP	LP	CP	LP	CP	LP	CP	LP	CP	LP	CP	LP	CP	LP	CP	LP	CP				
A	4.1	7	13	10	18	4.7 ± 0.9	4.7 ± 0.7	10.4 ± 0.6	18.2 ± 1.6	6.6 ± 0.2	10.9 ± 0.7	10.5 ± 1.2	4.8 ± 1.0	182 ± 6	182 ± 6	1.62 ± 3																					
B	4.4	3	2	8	6	9.9 ± 1.9	19.6 ± 4.0	12.4 ± 1.0	19.7 ± 0.6	8.2 ± 0.6	12 ± 2.0	46.8 ± 1.9	33.5 ± 3.8	200 ± 7	200 ± 7	1.74 ± 4																					
C	3.6	8	8	9	11	23.2 ± 1.3	21.6 ± 2.0	11.6 ± 0.5	18.2 ± 0.9	7.3 ± 0.5	11.2 ± 1.2	49 ± 2.0	13 ± 2.9	212 ± 11	212 ± 11	1.93 ± 5																					
D	4.1	7	8	8	9	4 ± 0.8	5.5 ± 1.4	11.5 ± 0.8	18.7 ± 2.4	7.1 ± 0.4	10.7 ± 1.9	4.7 ± 1.3	5.5 ± 2.2	207 ± 7	207 ± 7	1.59 ± 4																					
Average						10.1 ± 1.9	12.9 ± 1.5	11.5 ± 0.4	18.4 ± 0.9	7.2 ± 0.2	10.9 ± 0.6	27.3 ± 7.8	10.8 ± 3.1	200 ± 6	200 ± 6	1.70 ± 5																					

ϕ_y) in FWHM is larger for CP ($\langle \phi_x \rangle = 18.4$ mrad, $\langle \phi_y \rangle = 10.9$ mrad) than for LP ($\langle \phi_x \rangle = 11.5$ mrad, $\langle \phi_y \rangle = 7.2$ mrad). Thus, the electron beam generated during LWFA via CP exhibits an increased divergence. This is because the electrons ionized and injected by CP laser pulses gain larger transverse momenta than by LP. In addition, the electrons produced under CP follow helical trajectories, as also observed in self-injection [27,28], which further enhances the beam divergence. It is interesting to note that both LP and CP cases exhibit an asymmetric transverse (x - y) distribution. This asymmetry can be attributed to the characteristics of the laser system used in the experiment. The laser system displays a large asymmetric pointing distribution in the x and y directions, as shown in Fig. 3(c), which influences the transverse distribution of the electrons in both the LP and CP cases.

The reproducibility of electron beams was also compared for LP and CP. The success rate of electron acceleration was 58% (88 out of 153 shots) for CP and 31% (247 out of 807 shots) for LP. These results indicate that CP provides a significantly higher reproducibility rate, approximately 2 times higher than for LP. This improvement can be ascribed to the superior capability of CP in producing and injecting more charge during LWFA. It enhances the likelihood of producing an electron beam, even in the presence of shot-to-shot variations in many laser-plasma parameters.

We also compared the electron charge and energy for LP and CP, utilizing measurements from the Lanex 1 and Lanex 3 detectors. Figure 3(d), derived from the electron-beam profiles observed on Lanex 1, reveals a remarkable difference in the total charge for CP and LP in all energy ranges. Specifically, CP exhibits a significantly higher total charge, with an average increase up to 30% compared to LP. We note that some CP shots yielded less charge counts than LP ones, especially at high gas densities. This is because part of the electron beam was clipped when detected on Lanex 1 due to its larger beam pointing and divergence in the CP case.

However, the charge detected on Lanex 3, covering electron energies above 120 MeV, is higher for LP than CP, as shown in Fig. 3(e). Furthermore, we measured the peak energy of the electron beam observed on Lanex 3. In Figure 3(f), the averaged electron peak energy is plotted as a function of the plasma density. The results show that the peak energy is higher for LP than CP in most cases. This is explained in Sec. III.

III. SIMULATIONS

To better understand the physics behind the influence of laser polarization on electron acceleration in LWFA, we performed PIC simulations using the SMILEI code [37], using Fourier decomposition with three azimuthal modes ($m = 0, 1$, and 2) in cylindrical geometry. Specifically, we

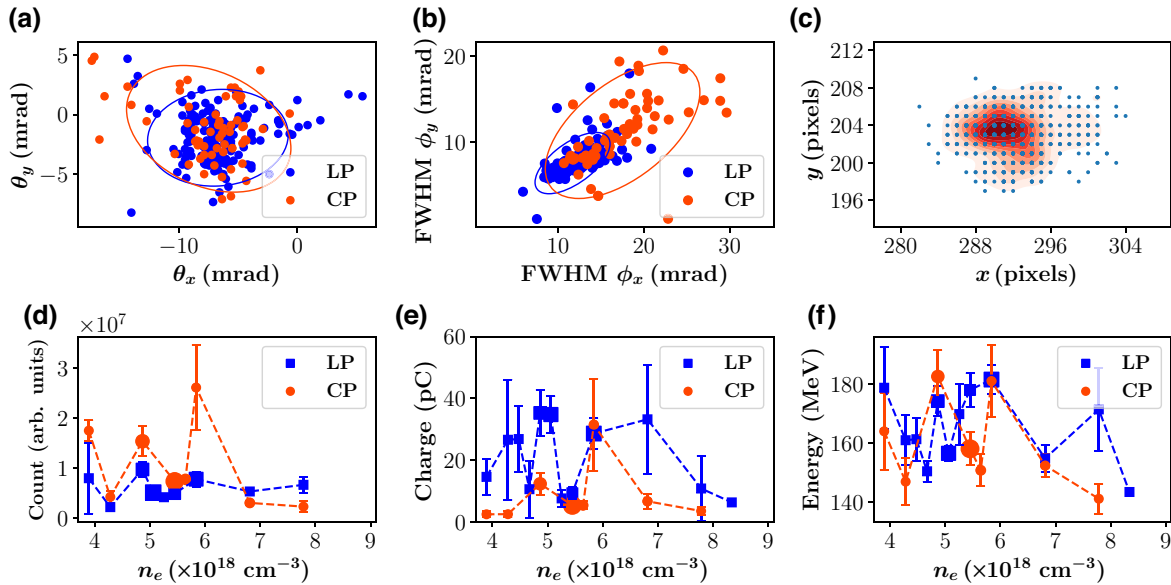


FIG. 3. (a) Electron-beam-pointing fluctuations detected on Lanex 1 for LP (blue scatters) and CP (red scatters) with covariance confidence ellipses added. (b) Electron-beam divergence (FWHM) in the transverse (x and y) directions on Lanex 1 with covariance confidence ellipses added. (c) A map of the laser- (far-field) beam-pointing fluctuations in the x and y directions, after the compressor, captured with 1416 laser shots. (d),(e) The average (d) count on Lanex 1 and (e) charge on Lanex 3, respectively, versus the plasma density. (f) The mean peak energy of electron beams on Lanex 3 versus the plasma density. In (d)–(f), the size of the scatters represents the number of shots.

studied the interaction between a Gaussian laser pulse ($a_0 = 1.5$, $w_0 = 20 \mu\text{m}$, $\tau = 27 \text{ fs}$, and $\lambda = 800 \text{ nm}$), first propagating in vacuum over $30 \mu\text{m}$, and a gaseous medium with a nonuniform density profile consisting of a 1-mm up-ramp, a 2-mm plateau, and a 1-mm down-ramp. This structure resembles our measurement. We used a moving window, propagating at the group velocity of the laser, with dimensions of $4\lambda_p \times 15\lambda_p$ divided by 2112×1216 cells (16 particles per cell) in the z and r directions. The simulations were performed for three types of target species—preionized He plasma, pure He gas, and 97% He with 3% N₂ (He–3% N₂). The ionization rate is calculated using the Ammosov-Delone-Krainov (ADK) model implemented in the SMILEI code.

The electron-density profile after about 2-mm propagation of the laser pulse is shown in Fig. 4 for each medium. The corresponding energy density is plotted in the inset. In the case of the preionized He driven with LP and CP [see Figs. 4(a) and 4(d)], they show an almost identical wakefield structure, as the ponderomotive force is polarization independent and there is no ionization involved. In the He case, we observe a slight modification in the electron energy density distribution. However, for He–3% N₂, the wakefield structure changes dramatically because of strong polarization-dependent ionization with N₂. With CP in particular, the electrons acquire higher residual longitudinal momenta, so that the probability of an electron being born

in a trapped orbit increases [14]. We also find that the spatial distribution of the beam charge and energy is wider for CP than for LP, which confirms the larger beam divergence for CP.

The corresponding phase-space profiles in the transverse direction are shown in Figs. 5(a)–5(f). For all gas species, the accelerated electrons have larger momenta in the transverse (y) direction for CP than for LP. In addition, the phase-space distribution changes dramatically with polarization; in particular, with the ionization-injection scheme (He–3% N₂). This is more evident around $y = 0$. If we look at the final electron spectrum shown in Figs. 5(g)–5(i), the peak energy is higher for LP in all cases. In the case of preionized plasma and He gas, there is a slightly higher peak energy for LP but the difference is not considered significant. On the other hand, for He–3% N₂, the difference in the peak energy between CP and LP is more pronounced. The energy spread of the main electron beam tends to increase with both LP and CP in the case of He–3% N₂. The main peak energy in the preionized He plasma is 240 MeV and 260 MeV for LP and CP, respectively. In He–3% N₂, the main peak energy is around 190 MeV and 130 MeV for LP and CP, respectively. In addition, there is a small peak around 380 MeV in preionized He plasma for LP. This peak decreases to 355 MeV and 204 MeV for LP and CP in He–3% N₂. The simulation results show, for both cases, that the total charge for CP is

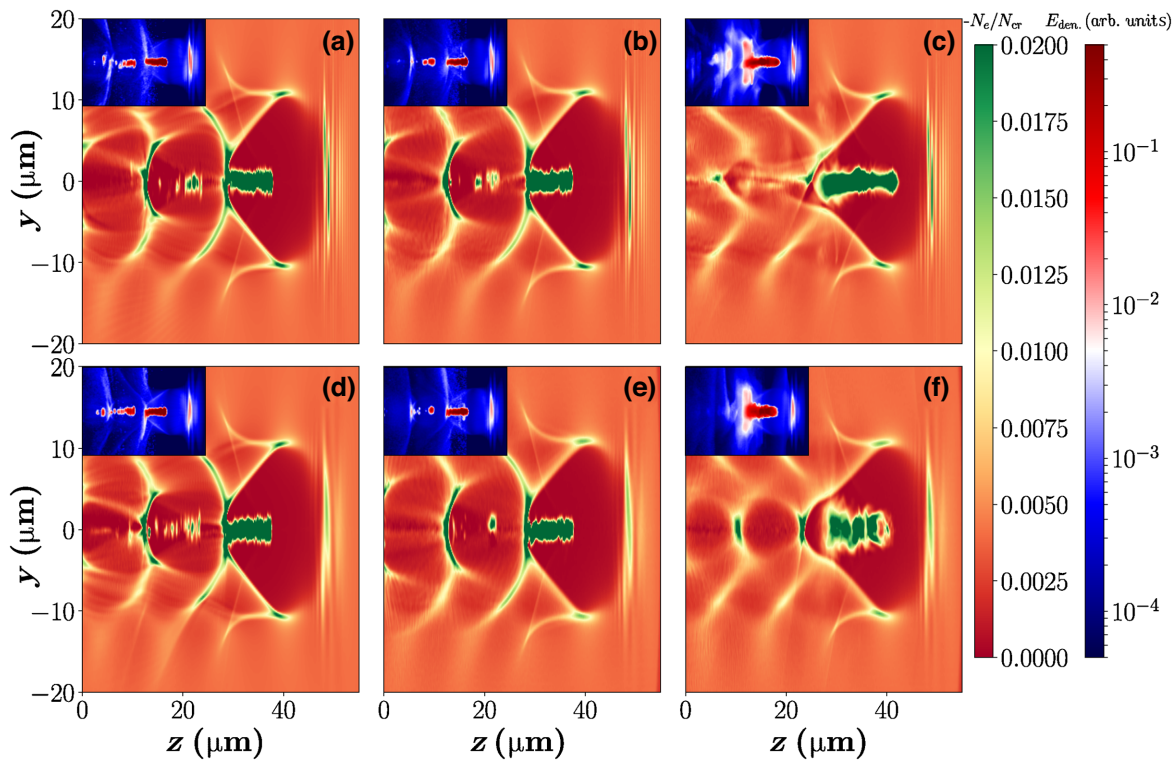


FIG. 4. The electron density (the inset shows the energy density of the electrons) after a 2-mm propagation of the laser pulse [(a)–(c) LP, (d)–(f) CP] in (a),(d) preionized He plasma, (b),(e) pure He, and (c),(f) 97% He with 3% N₂.

higher than for LP, and the charge of the electrons above 120 MeV is higher for LP than for CP, which confirms our experimental results.

Our simulation results also show why LP yields higher electron energies than CP in the case of He–3% N₂. The evolution of plasma densities, shown in Fig. 4(c) and in Figs. S.2–S.6 in the Supplemental Material [33], indicates that in the case of LP, the injected electron bunch is narrower and extends to the back of the bubble. In the CP case, however, there is a noticeably large gap between the electron bunch and the back of the bubble. This is due to ionization injection that is sensitive to the polarization of the driver laser. The ionization of the *K* shell of nitrogen occurs earlier in time for an LP laser pulse because of its higher a_0 compared to the CP case. The electrons born early in time can be injected close to the back of the cavity (similar to self-injection), where the longitudinal wakefield is stronger and can produce higher electron energies. From the ADK model and also our simulation, we note that N⁶⁺ is formed at the peak of an LP laser pulse with $a_0 = 1.4$, whereas almost no N⁶⁺ is produced with CP. With relativistic self-focusing and thereby an increasing a_0 , both polarization states can produce N⁶⁺ and N⁷⁺.

However, LP always yields the higher a_0 at any evolution time and can inject electrons closer to the back of the plasma bubble compared to CP. This can produce higher-energy spectra. The general enhancement of total charge with CP can be also explained by PIC simulations. First, our PIC simulation results show that the minimum of the wake potential [4,14] decreases further with CP (see Fig. S.7 in the Supplemental Material [33]) and this effectively increases the Hamiltonian on the separatrix (or decreases the threshold for trapping) [14]. As a result, a higher number of electrons can be trapped, ultimately leading to an increased total charge. Second, the electrons ionized and accelerated by a CP laser pulse can gain higher longitudinal momenta [27,28,38]. This also lowers the threshold for trapping [14,39], which can yield more charge in the beam.

IV. CONCLUSIONS

In conclusion, our findings highlight the significant influence of polarization-dependent ionization injection in LWFA. Its primary contributions are twofold. First, the laser polarization determines the residual momentum distribution of electrons when liberated via ATI.

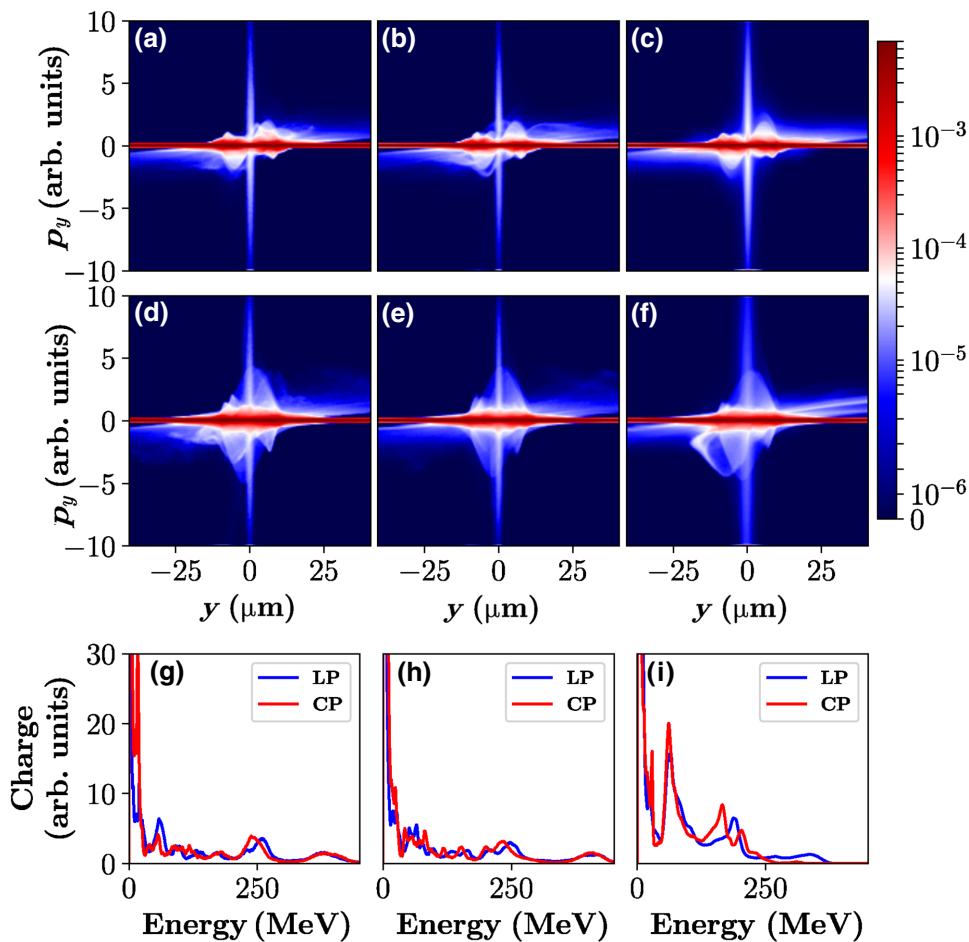


FIG. 5. The transverse phase-space distribution (p_y versus y) of the electron beam (first row, LP; second row, CP) after a 2.6-mm propagation of the laser pulse in (a),(d) preionized He plasma, (b),(e) pure He gas, and (c),(f) 97% He mixed with 3% N₂. (g)–(i) Electron spectra at the end of laser propagation in (g) preionized He plasma, (h) pure He gas, and (i) He–3% N₂, for LP (blue line) and CP (red line).

This affects the subsequent behavior and dynamics of ionization-injected electrons. Second, given the same laser energy, pulse duration, and focal spot, the polarization state changes the peak laser intensity. This can alter the onset of the ionization time, consequently changing the trajectories of ionization-injected electrons in the phase space. Our experimental results show that CP tends to increase the electron reproducibility rate (by 90%), the electron-beam divergence (by 60%), and the total electron charge (up to 30%) compared to LP, while LP provides the higher peak electron energy (by 20%) and slightly less electron-beam-pointing fluctuation. The results, also supported by 3D PIC simulations, reveal the potential of laser polarization as an additional tuning knob for LWFA, opening up new opportunities for more controllable LWFA depending on applications. In addition, the study of CP laser interaction with plasma is important, as it can generate tunable magnetic fields [40] and circularly polarized x rays [41] with increased charge and radiation power, also improving the conversion efficiency with higher success rates.

The data that support the findings of this study are available from the corresponding author upon reasonable request.

ACKNOWLEDGMENTS

This work was supported by the Institute for Basic Science under IBS-R012D1. We gratefully acknowledge S. Cho and J. Jeon for technical assistance with the experimental setups. We acknowledge the laser team at CoReLS for their support of the laser operation and for maintenance and W. S. Bang's group for their work on the gas-jet characterization. We thank F. Pérez and F. Massimo from the SMILEI team for their helpful insights regarding the PIC simulation. The computational works for this research were performed on the IBS Supercomputer, Aleph, in the IBS Research Solution Center.

- [1] M. D. Perry and G. Mourou, Terawatt to petawatt subpicosecond lasers, *Science* **264**, 917 (1994).
- [2] V. Malka, Laser plasma accelerators, *Phys. Plasmas* **19**, 055501 (2012).
- [3] T. Tajima and J. M. Dawson, Laser Electron Accelerator, *Phys. Rev. Lett.* **43**, 267 (1979).
- [4] J. Wenz and S. Karsch, Physics of laser-wakefield accelerators (LWFA), arXiv preprint [ArXiv:2007.04622](#) (2020).
- [5] K. Nakajima, Laser-driven plasma electron acceleration and radiation, *Rev. Accel. Sci. Technol.* **09**, 19 (2016).
- [6] T. Tajima and K. Homma, Fundamental physics explored with high intensity laser, *Int. J. Mod. Phys. A* **27**, 1230027 (2012).
- [7] S. Banerjee, S. Y. Kalmykov, N. D. Powers, G. Golovin, V. Ramanathan, N. J. Cunningham, K. J. Brown, S. Chen, I. Ghebregziabher, B. A. Shadwick, D. P. Umstadter, B. M. Cowan, D. L. Bruhwiler, A. Beck, and E. Lefebvre, Stable, tunable, quasimonoenergetic electron beams produced in a

laser wakefield near the threshold for self-injection, *Phys. Rev. Spec. Top.—Accel. Beams* **16**, 031302 (2013).

- [8] F. Albert and A. G. Thomas, Applications of laser wakefield accelerator-based light sources, *Plasma Phys. Controlled Fus.* **58**, 103001 (2016).
- [9] R. Dey and A. C. Roy, Inverse bremsstrahlung heating rate for dense plasmas in laser fields, *Phys. Plasmas* **20**, 073108 (2013).
- [10] C. I. Hojbotá, M. Mirzaie, D. Y. Kim, T. G. Pak, M. Rezaei-Pandari, V. B. Pathak, J. H. Jeon, J. W. Yoon, J. H. Sung, and S. K. Lee, High-energy betatron source driven by a 4-pW laser with applications to non-destructive imaging, arXiv preprint [ArXiv:2211.07963](#) (2022).
- [11] T. Pak, M. Rezaei-Pandari, S. B. Kim, G. Lee, D. H. Wi, C. I. Hojbotá, M. Mirzaie, H. Kim, J. H. Sung, S. K. Lee, C. Kang, and K.-Y. Kim, Multi-millijoule terahertz emission from laser-wakefield-accelerated electrons, *Light: Sci. Appl.* **12**, 37 (2023).
- [12] W. Lu, Ph.D. thesis, University of California, Los Angeles (2006).
- [13] E. Esarey and M. Pilhoff, Trapping and acceleration in nonlinear plasma waves, *Phys. Plasmas* **2**, 1432 (1995).
- [14] J. Faure, Plasma injection schemes for laser-plasma accelerators, arXiv preprint [ArXiv:1705.10542](#) (2017).
- [15] S. Kalmykov, S. A. Yi, V. Khudik, and G. Shvets, Electron Self-Injection and Trapping into an Evolving Plasma Bubble, *Phys. Rev. Lett.* **103**, 135004 (2009).
- [16] D. L. Bruhwiler, D. A. Dimitrov, J. R. Cary, E. Esarey, W. Leemans, and R. E. Giaccone, Particle-in-cell simulations of tunneling ionization effects in plasma-based accelerators, *Phys. Plasmas* **10**, 2022 (2003).
- [17] C. McGuffey, A. G. R. Thomas, W. Schumaker, T. Matsuoka, V. Chvykov, F. J. Dollar, G. Kalintchenko, V. Yanovsky, A. Maksimchuk, K. Krushelnick, V. Y. Bychenkov, I. V. Glazyrin, and A. V. Karpeev, Ionization Induced Trapping in a Laser Wakefield Accelerator, *Phys. Rev. Lett.* **104**, 025004 (2010).
- [18] B. Marchetti, R. Assmann, U. Dorda, and J. Zhu, Conceptual and technical design aspects of accelerators for external injection in LWFA, *Appl. Sci.* **8**, 757 (2018).
- [19] J. Hua, Y. Wu, and W. Lu, External injection from a Linac into a LWFA with ~100% capture efficiency (SPIE, 2019), p. 110370V.
- [20] S. A. Yi, V. Khudik, S. Y. Kalmykov, and G. Shvets, Hamiltonian analysis of electron self-injection and acceleration into an evolving plasma bubble, *Plasma Phys. Controlled Fus.* **53**, 014012 (2010).
- [21] C. Benedetti, C. B. Schroeder, E. Esarey, F. Rossi, and W. P. Leemans, Numerical investigation of electron self-injection in the nonlinear bubble regime, *Phys. Plasmas* **20**, 103108 (2013).
- [22] H. Xu, W. Yu, P. Lu, V. K. Senecha, F. He, B. Shen, L. Qian, R. Li, and Z. Xu, Electron self-injection and acceleration driven by a tightly focused intense laser beam in an underdense plasma, *Phys. Plasmas* **12**, 013105 (2005).
- [23] K. Schmid, A. Buck, C. M. S. Sears, J. M. Mikhailova, R. Tautz, D. Herrmann, M. Geissler, F. Krausz, and L. Veisz, Density-transition based electron injector for laser driven wakefield accelerators, *Phys. Rev. Spec. Top.—Accel. Beams* **13**, 091301 (2010).

- [24] C. Wang, J. Li, J. Sun, and X. Luo, Shock-wave-based density down ramp for electron injection, *Phys. Rev. Spec. Top.—Accel. Beams* **15**, 020401 (2012).
- [25] C. Aniculaesei, V. B. Pathak, K. H. Oh, P. K. Singh, B. R. Lee, C. I. Hojbota, T. G. Pak, E. Brunetti, B. J. Yoo, J. H. Sung, S. K. Lee, H. T. Kim, and C. H. Nam, Proof-of-Principle Experiment for Nanoparticle-Assisted Laser Wakefield Electron Acceleration, *Phys. Rev. Appl.* **12**, 044041 (2019).
- [26] A. Jain and D. N. Gupta, Improvement of electron beam quality in laser wakefield acceleration by a circularly-polarized laser pulse, *Plasma Phys. Controlled Fus.* **63**, 075007 (2021).
- [27] Y. Ma, D. Seipt, A. Hussein, S. Hakimi, N. Beier, S. Hansen, J. Hinojosa, A. Maksimchuk, J. Nees, K. Krushelnick, A. Thomas, and F. Dollar, Polarization-Dependent Self-Injection by Above Threshold Ionization Heating an a Laser Wakefield Accelerator, *Phys. Rev. Lett.* **124**, 114801 (2020).
- [28] Y. Ma, D. Seipt, A. E. Hussein, S. Hakimi, N. F. Beier, S. B. Hansen, J. Hinojosa, A. Maksimchuk, J. Nees, and K. Krushelnick, The effects of laser polarization and wavelength on injection dynamics of a laser wakefield accelerator, *Phys. Plasmas* **28**, 063101 (2021).
- [29] P. Kumar, K. Yu, R. Zgadzaj, M. Downer, I. Petrushina, R. Samulyak, V. Litvinenko, and N. Vafaei-Najafabadi, Evolution of the self-injection process in long wavelength infrared laser driven LWFA, *Phys. Plasmas* **28**, 013102 (2021).
- [30] M. Mirzaie, G. Zhang, S. Li, K. Gao, G. Li, Q. Ain, and N. A. Hafz, Effect of injection-gas concentration on the electron beam quality from a laser-plasma accelerator, *Phys. Plasmas* **25**, 043106 (2018).
- [31] Q. Ain, N. A. Hafz, S. Li, M. Mirzaie, K. Gao, G. Li, and J. Zhang, Laser wakefield acceleration in Kr-He plasmas and its application to positron beam generation, *Plasma Phys. Controlled Fus.* **60**, 085012 (2018).
- [32] M. Mirzaie, N. A. Hafz, S. Li, F. Liu, F. He, Y. Cheng, and J. Zhang, Enhanced electron yield from laser-driven wakefield acceleration in high-Z gas jets, *Rev. Sci. Instrum.* **86**, 103502 (2015).
- [33] See the Supplemental Material at <http://link.aps.org-supplemental/10.1103/PhysRevApplied.20.034026>, for comprehensive analyses of the gas density, plasma evolution, electric fields, and wake potential in the medium.
- [34] C. I. Hojbota, H. T. Kim, J. H. Shin, C. Aniculaesei, B. S. Rao, and C. H. Nam, Accurate single-shot measurement technique for the spectral distribution of GeV electron beams from a laser wakefield accelerator, *AIP Adv.* **9**, 085229 (2019).
- [35] S. Singh, T. Slavicek, R. Hodak, R. Versaci, P. Pridal, and D. Kumar, Absolute calibration of imaging plate detectors for electron kinetic energies between 150 keV and 1.75 MeV, *Rev. Sci. Instrum.* **88**, 075105 (2017).
- [36] N. Nakanii, K. Kondo, T. Yabuuchi, K. Tsuji, K. Tanaka, S. Suzuki, T. Asaka, K. Yanagida, H. Hanaki, and T. Kobayashi, *et al.*, Absolute calibration of imaging plate for GeV electrons, *Rev. Sci. Instrum.* **79**, 066102 (2008).
- [37] J. Derouillat, A. Beck, F. Pérez, T. Vinci, M. Chiaramello, A. Grassi, M. Flé, G. Bouchard, I. Plotnikov, N. Aunai, J. Dargent, C. Riconda, and M. Grech, SMILEI: A collaborative, open-source, multi-purpose particle-in-cell code for plasma simulation, *Comput. Phys. Commun.* **222**, 351 (2018).
- [38] J. Vieira, J. Martins, and U. Sinha, Plasma based helical undulator for controlled emission of circularly and elliptically polarised betatron radiation, arXiv preprint [ArXiv:1601.04422](https://arxiv.org/abs/1601.04422) (2016).
- [39] K. Marsh, C. E. Clayton, C. Joshi, W. Lu, W. B. Mori, A. Pak, N. Lemos, R. Fonseca, S. de Freitas, and F. Albert, *et al.*, *Laser wakefield acceleration beyond 1 GeV using ionization induced injection*, Tech. Rep. [Lawrence Livermore National Laboratory (LLNL), Livermore, California, 2011].
- [40] M. Lamač, U. Chaulagain, J. Nejdl, and S. V. Bulanov, Generation of intense magnetic wakes by relativistic laser pulses in plasma, *Sci. Rep.* **13**, 1701 (2023).
- [41] J. Feng, Y. Li, X. Geng, D. Li, J. Wang, M. Mirzaie, and L. Chen, Circularly polarized x-ray generation from an ionization induced laser plasma electron accelerator, *Plasma Phys. Controlled Fus.* **62**, 105021 (2020).